

Classical-quantum correspondence of special and extraordinary-log criticality: Villain's bridge

Yanan Sun,¹ Jin Lyu,¹ and Jian-Ping Lv^{1,*}

¹Anhui Key Laboratory of Optoelectric Materials Science and Technology,
Key Laboratory of Functional Molecular Solids, Ministry of Education,
Anhui Normal University, Wuhu, Anhui 241000, China

(Dated: December 6, 2022)

There has been much recent progress on exotic surface critical behavior, yet the classical-quantum correspondence of special and extraordinary-log criticality remains largely unclear. Employing worm Monte Carlo simulations, we explore the surface criticality at an emergent superfluid-Mott insulator critical point in the Villain representation, which is believed to connect classical and quantum O(2) critical systems. We observe a special transition with the thermal and magnetic renormalization exponents $y_t = 0.58(1)$ and $y_h = 1.690(1)$ respectively, which are close to recent estimates from models with discrete spin variables. The existence of extraordinary-log universality is evidenced by the critical exponent $\hat{q} = 0.58(2)$ from two-point correlation and the renormalization-group parameter $\alpha = 0.28(1)$ from superfluid stiffness, which obey the scaling relation of extraordinary-log critical theory and recover the logarithmic finite-size scaling of critical superfluid stiffness in open-edge quantum Bose-Hubbard model. Our results bridge recent observations of surface critical behavior in the classical statistical mechanical models [Parisen Toldin, Phys. Rev. Lett. **126**, 135701 (2021); Hu *et al.*, *ibid.* **127**, 120603 (2021); Parisen Toldin *et al.*, *ibid.* **128**, 215701 (2022)] and the open-edge quantum Bose-Hubbard model [Sun *et al.*, Phys. Rev. B **106**, 224502 (2022)].

I. INTRODUCTION

Surface criticality (SC) refers to the critical behavior occurring on open surfaces of a critical system. For decades, SC has been a fundamental topic for modern critical theory [1–15]. Direct relevance has been established from SC to state-of-the-art topics including the surface effects of symmetry-protected topological phase [16–18], critical Casimir effects [19], boundary conformal field [20, 21], numerical conformal bootstrap [22] and logarithmic critical scaling [23–25].

The O(N) systems—including the self-avoiding random walk ($N = 0$), Ising ($N = 1$), XY ($N = 2$) and Heisenberg ($N = 3$) models—serve as a prototypical platform for the ubiquity of criticality. Indeed, they host nontrivial SC such as the special transition and extraordinary critical phase associated with the ordinary critical phase [4–6, 9, 15, 22–24]. The characteristics of SC depend on N and the space-time dimension $D = d + z$, with d the spatial dimension and z the dynamic critical exponent. Present work focuses on $D = 3$.

Figure 1 displays the phase diagram of SC for $N = 2$, where the special transition is a multi-critical point terminating the Kosterlitz-Thouless-type surface transition line and separating the ordinary and extraordinary critical phases [6, 24]. The phase diagram is therefore divided into order and disorder regimes for both surface and bulk, as well as a regime of quasi-long-range ordered surface in presence of a disordered bulk. Recently, O(2) special transitions were also found in the classical three-state Potts antiferromagnet [26] and six-state clock model [27] as well as the two-dimensional quantum Bose-Hubbard model [28]—each of them can be accounted for by an emergent bulk O(2) criticality. As summarized in Table I, however, the estimates for the magnetic renormalization exponent y_h from different contexts are not fully consistent.

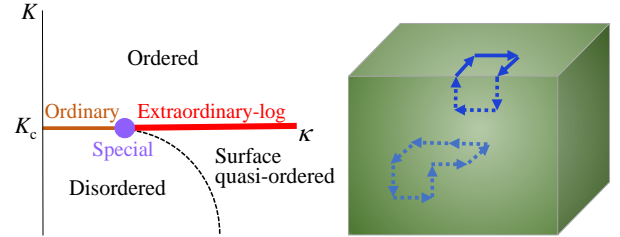


Figure 1. Left panel: The phase diagram of O(2) surface criticality in terms of the bulk interaction K and the ratio κ of surface interaction enhancement [6, 15, 28]. Right panel: Illustration for the open-surface Villain model, displaying two closed loops of directed flows. The directed flows on open surfaces have a distinct statistical weight from that in bulk.

The critical behavior of the extraordinary phase at $N = 2$ has been a long-standing controversy [6, 15]. The theory of extraordinary-log universality (ELU) was recently proposed for $2 \leq N < N_c$ [15], with N_c an unknown upper bound. In this scenario, the surface two-point correlation $g(r)$ decays logarithmically with the spatial distance r as [15]

$$g(r) \sim (\ln r)^{-\hat{\eta}}, \quad (1)$$

where the exponent $\hat{\eta}$ merely depends on N . Numerical evidence for the existence of ELU has been obtained from critical Heisenberg [23] and XY [24, 25] models. Motivated by the Fourier-mode-dependent finite-size scaling (FSS) of magnetic fluctuations [29, 30] and the two-length scenarios in different contexts of bulk criticality [31–36], an alternative scaling form of $g(r)$ was conjectured [24] for ELU. This conjecture is based on the L dependence (L is linear size) of critical magnetic fluctuations at zero and smallest non-zero modes, which scale as $L^2(\ln L)^{-\hat{q}}$ and $L^2(\ln L)^{-\hat{\eta}}$ with the exponents \hat{q} and

* jplv2014@ahnu.edu.cn

Table I. Universal information for the O(2) surface criticality, including the renormalization exponents y_t (thermal) and y_h (magnetic) for the special transition, as well as the critical exponent \hat{q} and the renormalization-group parameter α for the extraordinary-log critical phase.

Special transition				
Reference	Year	Model	y_t	y_h
[6]	2005	XY model	0.608(4)	1.675(1)
[26]	2022	three-state antiferromagnetic Potts model	0.59(1)	1.693(2)
[27]	2022	six-state clock model	0.61(2)	1.688(1)
present work	2022	Villain model	0.58(1)	1.690(1)
Extraordinary-log critical phase				
Reference	Year	Model	\hat{q}	α
[24]	2021	XY model	0.59(2)	0.27(2)
[25]	2021	improved O(2) ϕ^4 model		0.300(5)
[26]	2022	three-state antiferromagnetic Potts model	0.60(2)	
[27]	2022	six-state clock model	0.59(1), 0.60(3), 0.59(3)	0.26(2), 0.24(4), 0.30(3)
present work	2022	Villain model	0.58(2)	0.28(1)

$\hat{\eta} = \hat{q} + 1$, respectively. The critical scaling behavior of $g(r)$ is described by [24]

$$g(r) \sim \begin{cases} (\ln r)^{-\hat{\eta}}, & \ln r \leq \mathcal{O}[(\ln L)^{\hat{q}/\hat{\eta}}], \\ (\ln L)^{-\hat{q}}, & \ln r \geq \mathcal{O}[(\ln L)^{\hat{q}/\hat{\eta}}]. \end{cases} \quad (2)$$

For the $N = 2$ case, the first result of \hat{q} is $\hat{q} = 0.59(2)$ [24]. The coexistence of the exponents \hat{q} and $\hat{\eta}$ was confirmed in the context of the ELU in three-state Potts antiferromagnet [26]. Table I lists the results of \hat{q} from different contexts [25–27]. Recall the scaling formula proposed [15] for the helicity modulus Υ , which measures the response of a system to a twist in boundary conditions [37]. The FSS of Υ is written as

$$\Upsilon L \sim 2\alpha(\ln L) \quad (3)$$

with the universal renormalization-group parameter α . Further, the scaling relation between \hat{q} and α reads [15]

$$\hat{q} = \frac{N-1}{2\pi\alpha}. \quad (4)$$

This relation has been verified for critical Heisenberg [23] and XY [24] models as well as an emergent O(2) critical point [27] (Table I).

Despite the complementary evidence for classical ELU and the numerous efforts toward a quantum counterpart, the self-contained picture for classical-quantum correspondence remains badly awaited [15]. Motivated by the exotic surface effects of symmetry-protected topological phases, SC has been extensively studied in dimerized antiferromagnetic quantum Heisenberg and XXZ models [10–14, 38–40], yet the existence of quantum ELU is still controversial. Very recently, quantum O(2) SC was explored in an open-edge Bose-Hubbard model of interacting soft-core bosons, where quantum special transition and quantum ELU were observed [28].

To establish a direct classical-quantum correspondence of O(2) SC, we formulate an open-surface Villain (OSV) model and study the special transition and extraordinary-log critical phase. Such a methodology was applied to the linear-response dynamics at a quantum O(2) critical point [41]. The Villain

model can be viewed as a variant of the quantum phase model, which is connected with the unit-filling Bose-Hubbard model. The Hamiltonian of the Bose-Hubbard model reads [42]

$$\mathcal{H}_{\text{BH}} = -t \sum_{\langle \mathbf{r}\mathbf{r}' \rangle} (\hat{\Phi}_{\mathbf{r}}^\dagger \hat{\Phi}_{\mathbf{r}'} + \hat{\Phi}_{\mathbf{r}} \hat{\Phi}_{\mathbf{r}'}^\dagger) + \frac{U}{2} \sum_{\mathbf{r}} \hat{n}_{\mathbf{r}}^2 \quad (5)$$

where $\hat{\Phi}_{\mathbf{r}}^\dagger$ and $\hat{\Phi}_{\mathbf{r}}$ are the bosonic creation and annihilation operators at site \mathbf{r} respectively, $\hat{n}_{\mathbf{r}} = \hat{\Phi}_{\mathbf{r}}^\dagger \hat{\Phi}_{\mathbf{r}}$ is the particle number operator, t represents the strength of nearest-neighbor hopping, and U denotes onsite repulsion. The superfluid-Mott insulator transition of unit-filling Bose-Hubbard model belongs to emergent O(2) criticality [43]. By integrating out amplitude fluctuations, the quantum phase model is formally [44]

$$\mathcal{H}_{\text{QR}} = -t \sum_{\langle \mathbf{r}\mathbf{r}' \rangle} \cos(\hat{\phi}_{\mathbf{r}} - \hat{\phi}_{\mathbf{r}'}) + \frac{U}{2} \sum_{\mathbf{r}} \hat{n}_{\mathbf{r}}^2, \quad (6)$$

where $\hat{n}_{\mathbf{r}}$ is now the deviation from mean filling and t is a multiple of that in Eq. (5). $\hat{\phi}_{\mathbf{r}}$ is conjugate to $\hat{n}_{\mathbf{r}}$ by $\hat{n}_{\mathbf{r}} = (1/i)(\partial/\partial\hat{\phi}_{\mathbf{r}})$. Hence, the quantum phase model is rewritten in angle representation as [45]

$$\mathcal{H}_{\text{QR}} = -t \sum_{\langle \mathbf{r}\mathbf{r}' \rangle} \cos(\phi_{\mathbf{r}} - \phi_{\mathbf{r}'}) + \frac{U}{2} \sum_{\mathbf{r}} \left(\frac{1}{i} \frac{\partial}{\partial \phi_{\mathbf{r}}} \right)^2. \quad (7)$$

Using standard Suzuki-Trotter decomposition, the inverse temperature β is divided into slices with width $\Delta\tau$ and a path-integral representation can be established [45]. Further, the Villain approximation is performed for $\cos(\phi)$ term, which is reexpressed by periodic Gaussians as $\exp(t\Delta\tau \cos(\phi)) \rightarrow \exp(t\Delta\tau) \sum_n \exp(-\frac{1}{2}t\Delta\tau(\phi - 2\pi n)^2)$ with n an integer, hence the periodicity in ϕ is unaffected [46]. Finally, by employing Poisson summation, it can be shown that the ground-state energy equals the free energy of the classical Hamiltonian [45, 47]

$$\mathcal{H}_{\text{V}} = \frac{1}{2K} \sum_{\langle \mathbf{r}\mathbf{r}' \rangle}^{\Delta\mathcal{J}=0} \mathcal{J}_{\mathbf{r}\mathbf{r}'}^2, \quad (8)$$

where the parameter K relates to the ratio t/U . $\mathcal{J}_{\mathbf{r}\mathbf{r}'} \in \{\dots, -2, -1, 0, 1, 2, \dots\}$ parameterizes the integer-valued directed flow between nearest-neighbor sites \mathbf{r} and \mathbf{r}' . $\Delta\mathcal{J} = 0$ denotes the absence of source and sink for flows— $\forall \mathbf{r}$, $\mathcal{D}_{\mathbf{r}} = \sum_{\mathbf{r}'} \mathcal{J}_{\mathbf{r}\mathbf{r}'} = 0$. The model (8) harbors the superfluid-Mott insulator transition [41, 45, 48–51], while a rigorous analysis for massless bulk phase became available recently [52].

Recall the hopping enhancement on open edges of quantum Bose-Hubbard model [28]. Here, we formulate an OSV model, where the parameter K becomes tunable on open surfaces. Hence, the OSV model is a classical counterpart of open-edge quantum Bose-Hubbard model and a possible testbed for classical-quantum correspondence. Besides, the OSV model admits state-of-the-art worm Monte Carlo simulations, by which the correlation function and superfluid (SF) stiffness can be efficiently sampled.

II. MODEL

The Hamiltonian of the OSV model reads

$$\mathcal{H}_{\text{OSV}} = \sum_{\langle \mathbf{r}\mathbf{r}' \rangle} \frac{\mathcal{J}_{\mathbf{r}\mathbf{r}'}^2}{2K_{\mathbf{r}\mathbf{r}'}} \quad (9)$$

where the parameter $K_{\mathbf{r}\mathbf{r}'}$ is for the nearest-neighbor sites \mathbf{r} and \mathbf{r}' on simple-cubic lattices. We impose open boundary conditions along [001] (z) direction as well as periodic boundary conditions along [100] (x) and [010] (y) directions. Hence, there are a pair of open surfaces. We set $K_{\mathbf{r}\mathbf{r}'} = K'$ if \mathbf{r} and \mathbf{r}' are on the same open surface and $K_{\mathbf{r}\mathbf{r}'} = K_c = 0.333\,067\,04$ for other situations, with K_c the bulk critical point of model (8) determined previously by two of us and coworkers [53]. The surface enhancement of $K_{\mathbf{r}\mathbf{r}'}$ is parameterized by $\kappa = (K' - K_c)/K_c$. A directed-flow state for model (9) is illustrated by Fig. 1.

III. METHODOLOGY BASED ON A WORM MONTE CARLO ALGORITHM

We simulate model (9) with the side length L of simple-cubic lattice ranging from $L = 4$ to 256. To this end, we formulate a worm Monte Carlo algorithm along the lines of Ref. [54]. Similar formulations of Monte Carlo algorithms have been applied to Villain model [49, 53, 55] and other lattice models [56–58]. Here, the methodology contains three components: extending state space (Sec. III A), update scheme (Sec. III B) and sampling of quantities (Sec. III C).

Conclusions of present work are drawn on the basis of FSS analyses of Monte Carlo data, for which we employ least-squares fits. In the fits, we analyze the dependence of the residuals χ^2 on the cut-off size L_{\min} . In principle, the reasonable fit corresponds to the smallest L_{\min} for which χ^2 per degree of freedom (DoF) obeys $\chi^2/\text{DoF} = \mathcal{O}(1)$ and for which subsequently increasing L_{\min} do not induce a decrement of χ^2/DoF over a unit. Practically, by “reasonable” one means that $\chi^2/\text{DoF} \approx 1$.

A. Extending state space

The partition function of model (9) reads

$$\mathcal{Z}_{\text{OSV}} = \sum_{\Delta\mathcal{J}=0} \prod_{\langle \mathbf{r}\mathbf{r}' \rangle} e^{-\frac{\mathcal{J}_{\mathbf{r}\mathbf{r}'}^2}{2K_{\mathbf{r}\mathbf{r}'}}} \quad (10)$$

where the summation runs over states in the directed-flow state space. For later convenience, \mathcal{Z}_{OSV} is unbiasedly reformulated in an extended state space as

$$\mathcal{Z}'_{\text{OSV}} = \frac{1}{L^3} \sum_{\Delta\mathcal{J}=0; \{I, M\}_{3d}} \delta_{I, M} \prod_{\langle \mathbf{r}\mathbf{r}' \rangle} e^{-\frac{\mathcal{J}_{\mathbf{r}\mathbf{r}'}^2}{2K_{\mathbf{r}\mathbf{r}'}}} \quad (11)$$

or

$$\mathcal{Z}''_{\text{OSV}} = \frac{1}{L^2} \sum_{\Delta\mathcal{J}=0; \{I, M\}_{2d}} \delta_{I, M} \prod_{\langle \mathbf{r}\mathbf{r}' \rangle} e^{-\frac{\mathcal{J}_{\mathbf{r}\mathbf{r}'}^2}{2K_{\mathbf{r}\mathbf{r}'}}} \quad (12)$$

by including two additional degrees of freedom—in a state, the sites I and M are specified on the whole lattice [Eq. (11)] or an open surface [Eq. (12)]. The summations run over the states in extended state spaces. δ denotes the Kronecker delta function.

The simulated partition functions in extended state space read

$$\mathcal{Z}'_{\text{sim}} = \mathcal{Z}'_{\text{OSV}} + \lambda \mathcal{G}' \quad (13)$$

and

$$\mathcal{Z}''_{\text{sim}} = \mathcal{Z}''_{\text{OSV}} + \lambda \mathcal{G}'' \quad (14)$$

with

$$\mathcal{G}' = \frac{1}{L^3} \sum_{\Delta\mathcal{J}=0; \{I, M\}_{3d}} (1 - \delta_{I, M}) \prod_{\langle \mathbf{r}\mathbf{r}' \rangle} e^{-\frac{\mathcal{J}_{\mathbf{r}\mathbf{r}'}^2}{2K_{\mathbf{r}\mathbf{r}'}}} \quad (15)$$

and

$$\mathcal{G}'' = \frac{1}{L^2} \sum_{\Delta\mathcal{J}=0; \{I, M\}_{2d}} (1 - \delta_{I, M}) \prod_{\langle \mathbf{r}\mathbf{r}' \rangle} e^{-\frac{\mathcal{J}_{\mathbf{r}\mathbf{r}'}^2}{2K_{\mathbf{r}\mathbf{r}'}}} \quad (16)$$

respectively, where λ is tunable. The subspaces with $I \neq M$, denoted in following by S' and S'' , contribute to \mathcal{G}' and \mathcal{G}'' , respectively.

B. Update scheme

To simulate partition function (13), an update scheme can be designed through a biased random walk that obeys detailed balance, by moving I and M on simple-cubic lattice. The procedure starts with $I = M$ in original state space. As I (M) moves to a neighbor I_n (M_n), the flow on edge II_n (MM_n) will be updated by adding a unit directed flow from I to I_n (M_n to M). Such a movement continues. When $I \neq M$, the flows passing I and M are not conserved, i.e., $\mathcal{D}_I \neq 0$ and

$\mathcal{D}_M \neq 0$, and S' space is hit. When $I = M$, the original state space is hit again. Thus, a movement of I or M is either a step of random walk in S' space or between S' and original spaces. More precisely, a Monte Carlo microstep is described in **Algorithm 1**.

Algorithm 1 Global update.

1. If $I = M$, randomly and uniformly choose a new site I' and set $I = M = I'$, $\text{sign}(I) = 1$, $\text{sign}(M) = -1$.
2. Interchange $I \leftrightarrow M$ and $\text{sign}(I) \leftrightarrow \text{sign}(M)$ with probability $1/2$.
3. If I is on an open surface, exit present micro Monte Carlo step with the probability $1/6$ [59].
4. Randomly and uniformly choose a neighbor I_n of I .
5. Propose to move $I \rightarrow I_n$ by updating the flow \mathcal{J}_{II_n} to \mathcal{J}'_{II_n} :

$$\mathcal{J}'_{II_n} = \mathcal{J}_{II_n} + \text{sign}(I \rightarrow I_n)\text{sign}(I),$$

where $\text{sign}(I \rightarrow I_n) = \pm 1$, permanently parametrizing the flow direction along edge- II_n .

6. Accept the proposal with probability

$$P_{\text{acc}} = \min[1, e^{\frac{-(\mathcal{J}'_{II_n} - \mathcal{J}_{II_n})}{2\kappa'}}]$$

if I and I_n are on an open surface, and, for other situations, with

$$P_{\text{acc}} = \min[1, e^{\frac{-(\mathcal{J}'_{II_n} - \mathcal{J}_{II_n})}{2\kappa}}].$$

In line with partition function (14), we formulate a *supplementary* procedure to **Algorithm 1** by the random walk of I and M on a specified open surface, which is described in **Algorithm 2**. We emphasize that **Algorithm 2** itself is not ergodic.

Algorithm 2 Restricted update.

1. If $I = M$, randomly and uniformly choose a new site I' on a specified open surface and set $I = M = I'$, $\text{sign}(I) = 1$, $\text{sign}(M) = -1$.
2. Interchange $I \leftrightarrow M$ and $\text{sign}(I) \leftrightarrow \text{sign}(M)$ with probability $1/2$.
3. Randomly and uniformly choose a neighbor I_n on the same open surface of I .
4. Propose to move $I \rightarrow I_n$ by updating the flow \mathcal{J}_{II_n} to \mathcal{J}'_{II_n} :

$$\mathcal{J}'_{II_n} = \mathcal{J}_{II_n} + \text{sign}(I \rightarrow I_n)\text{sign}(I).$$

5. Accept the proposal with probability

$$P_{\text{acc}} = \min[1, e^{\frac{-(\mathcal{J}'_{II_n} - \mathcal{J}_{II_n})}{2\kappa'}}].$$

A closed loop of directed flow is superposed once I meets M , and closed loops can be consecutively superposed. The update scheme switches between **Algorithm 1** and **2**, when a fixed number of closed loops is generated.

Practically, parallel simulations are carried out and a large number of closed loops are created. Around the special transition point ($0.44 \leq \kappa \leq 0.4428$), the number of generated closed loops ranges from 2.03×10^{10} to 5.42×10^{11} for

$8 \leq L \leq 128$ and increases to 5.06×10^{11} at $L = 256$. In the deep extraordinary critical regime ($\kappa = 5$ and 10), the number ranges from 4.95×10^9 to 7.93×10^{10} for $8 \leq L \leq 128$ and reaches 5.28×10^{10} at $L = 256$. For each independent simulation, the initial one sixth of closed loops are used for thermalization.

C. Sampling of quantities

Extended state space. Using **Algorithm 2**, we sample the probability distribution of the distance between I and M , which is an unbiased estimator for the surface two-point correlation $g(r_1, r_2)$ [$g(0, 0) \equiv 1$]. In particular, we define

$$G_1 = [g(0, L/4) + g(L/4, 0)]/2 \quad (17)$$

and

$$G_2 = [g(0, L/2) + g(L/2, 0)]/2. \quad (18)$$

The surface susceptibility χ can be evaluated by the number n_s of worm steps between subsequent hits to the original state space. Accordingly, χ is defined by

$$\chi = \langle n_s \rangle. \quad (19)$$

Original state space. The following quantities are sampled in original state space. First, the winding probabilities are given by

$$R_x = \langle \mathcal{R}_x \rangle = \langle \mathcal{R}_y \rangle, \quad (20)$$

$$R_a = \langle 1 - (1 - R_x)(1 - R_y) \rangle, \quad (21)$$

$$R_2 = \langle \mathcal{R}_x \mathcal{R}_y \rangle, \quad (22)$$

for which $\mathcal{R}_\alpha = 1$ (resp. $\mathcal{R}_\alpha = 0$) corresponds to the event that directed flows wind (resp. do not wind) in the α direction of simple-cubic lattice. Hence, R_x , R_a and R_2 define the probabilities that the winding of directed flows exists in x direction, in at least one direction and in both x and y directions, respectively. More or less similar dimensionless quantities can also be defined for geometric percolation transitions [60–66]. The SF stiffness relates to winding number fluctuations as

$$\rho = \langle \mathcal{W}_x^2 + \mathcal{W}_y^2 \rangle / (2L), \quad (23)$$

with \mathcal{W}_x and \mathcal{W}_y the winding numbers in x and y directions, respectively.

Further, for an observable (say \mathcal{O}), we define its covariance with the surface energy ε_s as

$$C_O = \frac{1}{K^2} (\langle \mathcal{O} \varepsilon_s \rangle - \langle \mathcal{O} \rangle \langle \varepsilon_s \rangle) \quad (24)$$

with

$$\varepsilon_s = \frac{1}{2} \sum_{\langle \mathbf{r}\mathbf{r}' \rangle_s} \mathcal{J}_{\mathbf{r}\mathbf{r}'}, \quad (25)$$

where the summation runs over edges on an open surface. Accordingly, C_O equals to the derivative of $O = \langle \mathcal{O} \rangle$ with respect to K' .

IV. SPECIAL TRANSITION

A. Location

We locate the special transition by varying κ . Recall the application of dimensionless winding probabilities in flow representation for O(2) criticality [53, 55] as well as an analog in world-line representation for the quantum special transition of Bose-Hubbard model [28]. When a special transition occurs at κ_c , R ($R = R_x, R_a$) is assumed to scale as

$$R = \tilde{R}(\epsilon L^{y_t}) \quad (26)$$

around κ_c , where ϵ equals $\kappa - \kappa_c$, y_t denotes the thermal renormalization exponent, and \tilde{R} is a scaling function. Figures 2(a) and (b) respectively show R_x and R_a versus κ for $L = 32, 48, 64, 96, 128$ and 256 . Scale invariance is observed at $\kappa_c \approx 0.441$. A more precise result comes from least-squares fits of the Monte Carlo data to the expansion of Eq. (26)

$$R = R^* + a_1 \epsilon L^{y_t} + a_2 \epsilon^2 L^{2y_t} + b_1 L^{-\omega_1} + \dots \quad (27)$$

where R^* is a critical value, a_1 , a_2 and b_1 are non-universal constants, and $b_1 L^{-\omega_1}$ represents the leading finite-size corrections with correction exponent ω_1 . For R_x , when the four terms in right-hand side of Eq. (27) are all included, preferred fits with $\chi^2/\text{DoF} \approx 0.7$ are achieved and yield $0.44141(5)$ and $0.44140(8)$ for $L_{\min} = 8$ and 16 , respectively. Meanwhile, we obtain the estimates of ω_1 as $\omega_1 = 1.06(9)$ and $1.1(3)$. A close value of leading correction exponent— $\omega_1 = 1$ from irrelevant surface fields—has been applied to the special transitions with $N = 1$ [9] and $N = 3$ [23]. Despite these observations, for caution, we should be aware of the correction exponent $\omega_1 \approx 0.789$ originating from O(2) bulk irrelevant field [67]. A useful procedure is to increase L_{\min} gradually and monitor the stability of fitting results. In this process, the finite-size corrections become more and more negligible. When $\omega_1 = 1$ is fixed, we obtain $\kappa_c = 0.44144(3)$, $0.44143(4)$, $0.44141(5)$, $0.44142(7)$ and $0.44143(9)$ with $L_{\min} = 8, 16, 32, 48$ and 64 , respectively. In Fig. 2(b), the finite-size corrections for R_a are relatively weak; hence, we perform fits without incorporating any finite-size correction. Stable results are achieved for large L_{\min} . In particular, we obtain $\kappa_c = 0.44132(3)$, $0.44137(3)$, $0.44139(4)$, $0.44138(5)$ and $0.44140(6)$ for $L_{\min} = 32, 48, 64, 96$ and 128 respectively, with $0.5 \lesssim \chi^2/\text{DoF} \lesssim 1.0$.

Assume that the SF stiffness scales as

$$\rho = L^{2-D} \tilde{\rho}(\epsilon L^{y_t}) \quad (28)$$

with $D = 3$, which relates to the FSS of SF stiffness for quantum special transition [28] by $D = d + z$ ($d = 2, z = 1$). We perform fits according to the scaling ansatz

$$\rho = L^{-1}(a_0 + a_1 \epsilon L^{y_t} + a_2 \epsilon^2 L^{2y_t} + b_1 L^{-\omega_1} + \dots) \quad (29)$$

with a_0 a constant. From Table II, one finds that the estimates of κ_c are close to those from R_x and R_a . This finding is illustrated by Fig. 2(c) demonstrating the $(\rho L) - \kappa$ relation, where

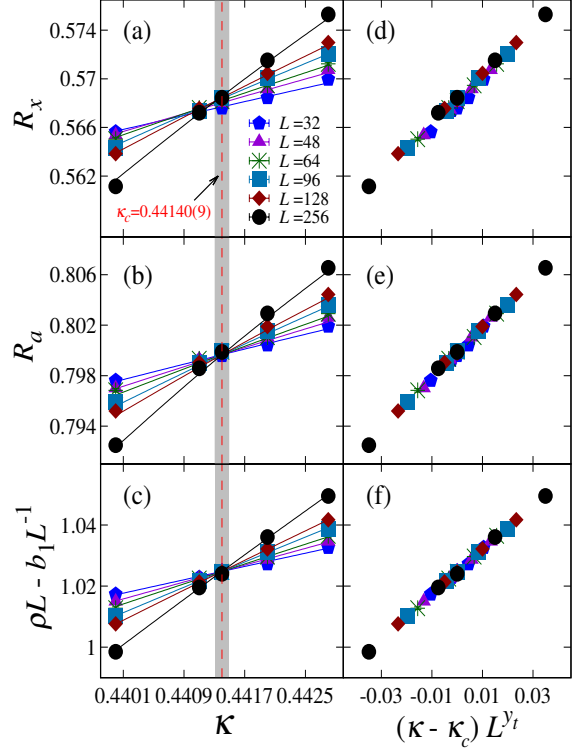


Figure 2. The winding probabilities R_x (a) and R_a (b) and the scaled SF stiffness $\rho L - b_1 L^{-1}$ (c) versus κ , where $b_1 = -0.329$ is taken from a preferred least-squares fit to Eq. (29). In panels (a), (b) and (c), the symbols stand for Monte Carlo data and the lines are drawn according to preferred fits. In panels (d), (e) and (f), the horizontal coordinates are set to be $(\kappa - \kappa_c) L^{y_t}$, with $\kappa_c = 0.44140$ and $y_t = 0.58$.

Table II. Fits of the winding probabilities R_x and R_a to Eq. (27) and the SF stiffness ρ to Eq. (29) for the special transition. “Q” is the abbreviation of sampled quantity and “—” indicates that the corresponding term is not included in fitting.

Q	L_{\min}	χ^2/DoF	κ_c	y_t	R^* or a_0	ω_1
R_x	8	23.81/33	0.44141(5)	0.59(1)	0.5687(2)	1.06(9)
	16	18.49/28	0.44140(8)	0.58(1)	0.5686(4)	1.1(3)
	8	24.23/34	0.44144(3)	0.59(1)	0.56884(8)	1
	16	18.61/29	0.44143(4)	0.58(1)	0.5688(1)	1
	32	17.35/24	0.44141(5)	0.58(2)	0.5687(2)	1
	48	11.19/19	0.44142(7)	0.59(2)	0.5687(3)	1
R_a	64	9.87/14	0.44143(9)	0.60(2)	0.5688(4)	1
	32	25.48/25	0.44132(3)	0.58(2)	0.79966(7)	—
	48	14.99/20	0.44137(3)	0.58(2)	0.79980(9)	—
	64	7.30/15	0.44139(4)	0.61(2)	0.7999(1)	—
	96	5.27/10	0.44138(5)	0.62(3)	0.7998(2)	—
	128	3.98/5	0.44140(6)	0.61(4)	0.7999(2)	—
ρ	8	45.76/34	0.44132(2)	0.59(1)	1.0235(3)	1
	16	20.35/29	0.44141(3)	0.58(1)	1.0248(4)	1
	32	16.40/24	0.44144(5)	0.58(1)	1.0253(7)	1
	48	9.41/19	0.44146(6)	0.57(2)	1.026(1)	1
	64	8.69/14	0.44146(8)	0.57(2)	1.026(2)	1

Table III. Fits of the covariances C_{R_x} , C_{R_a} , C_{R_2} and $C_{\rho L}$ to Eq. (31) at the special transition.

Q	L_{\min}	χ^2/DoF	a_0	y_t	b_1	ω_1
C_{R_x}	4	11.22/6	0.623(3)	0.570(1)	-0.13(1)	1
	8	6.68/5	0.611(6)	0.574(2)	-0.08(3)	1
	16	0.79/4	0.64(1)	0.566(4)	-0.28(9)	1
	16	10.84/5	0.600(3)	0.578(1)	—	—
	32	2.06/4	0.612(5)	0.573(2)	—	—
	48	0.42/3	0.619(8)	0.570(3)	—	—
C_{R_a}	4	24.58/6	0.642(4)	0.563(1)	-0.25(1)	1
	8	4.57/5	0.615(7)	0.572(3)	-0.11(3)	1
	16	1.07/4	0.64(1)	0.565(4)	-0.3(1)	1
	16	9.57/5	0.599(3)	0.577(1)	—	—
	32	1.06/4	0.614(6)	0.572(2)	—	—
	48	1.00/3	0.615(9)	0.571(3)	—	—
C_{R_2}	4	6.91/6	0.602(4)	0.577(2)	-0.01(1)	1
	8	6.69/5	0.605(7)	0.576(3)	-0.03(3)	1
	16	1.99/4	0.63(1)	0.568(5)	-0.2(1)	1
	16	7.43/5	0.599(3)	0.578(2)	—	—
	32	3.40/4	0.609(6)	0.574(3)	—	—
	48	0.29/3	0.62(1)	0.570(4)	—	—
$C_{\rho L}$	4	8.61/6	2.22(1)	0.576(1)	-0.94(3)	1
	8	8.48/5	2.23(2)	0.576(2)	-0.97(9)	1
	16	1.60/4	2.31(4)	0.569(3)	-1.7(3)	1
	16	39.32/5	2.097(9)	0.588(1)	—	—
	32	4.47/4	2.17(2)	0.580(2)	—	—
	48	0.30/3	2.21(3)	0.576(3)	—	—

Table IV. Fits of the two-point correlations G_1 and G_2 to Eq. (33) and the susceptibility χ to Eq. (34) at the special transition.

Q	L_{\min}	L_{\max}	χ^2/DoF	a_0	y_h	ω_1
G_1	8	256	2.55/4	1.54(2)	1.6888(9)	0.82(9)
	8	256	6.45/5	1.513(2)	1.6903(1)	1
	16	256	4.03/4	1.519(5)	1.6899(3)	1
	32	256	0.47/3	1.54(1)	1.6887(7)	1
	48	256	0.11/2	1.55(2)	1.688(1)	1
	8	128	1.73/3	1.53(2)	1.689(1)	0.9(1)
	8	128	3.78/4	1.512(2)	1.6904(1)	1
	16	128	2.46/3	1.517(5)	1.6900(4)	1
	32	128	0.18/2	1.53(1)	1.6889(8)	1
	48	128	0.05/1	1.54(3)	1.688(2)	1
G_2	8	256	14.01/4	1.27(2)	1.689(1)	0.9(1)
	8	256	14.60/5	1.261(2)	1.6901(2)	1
	16	256	14.20/4	1.264(5)	1.6899(4)	1
	32	256	13.50/3	1.27(1)	1.689(1)	1
	48	256	13.12/2	1.26(3)	1.690(3)	1
	8	128	4.95/3	1.27(1)	1.690(1)	0.9(1)
	8	128	5.16/4	1.261(2)	1.6901(2)	1
	16	128	4.98/3	1.263(5)	1.6900(4)	1
	32	128	4.73/2	1.27(1)	1.689(1)	1
	48	128	3.33/1	1.23(3)	1.692(3)	1
χ	8	256	3.28/4	1.45(1)	1.6894(7)	0.92(5)
	8	256	5.42/5	1.431(1)	1.6903(1)	1
	16	256	3.88/4	1.436(4)	1.6900(3)	1
	32	256	2.45/3	1.45(1)	1.6893(7)	1
	48	256	2.45/2	1.45(2)	1.689(2)	1
	8	128	0.75/3	1.44(1)	1.6895(7)	0.93(5)
	8	128	2.36/4	1.431(1)	1.6903(1)	1
	16	128	1.12/3	1.435(4)	1.6900(3)	1
	32	128	0.13/2	1.44(1)	1.6894(7)	1
	48	128	0.02/1	1.44(3)	1.690(2)	1

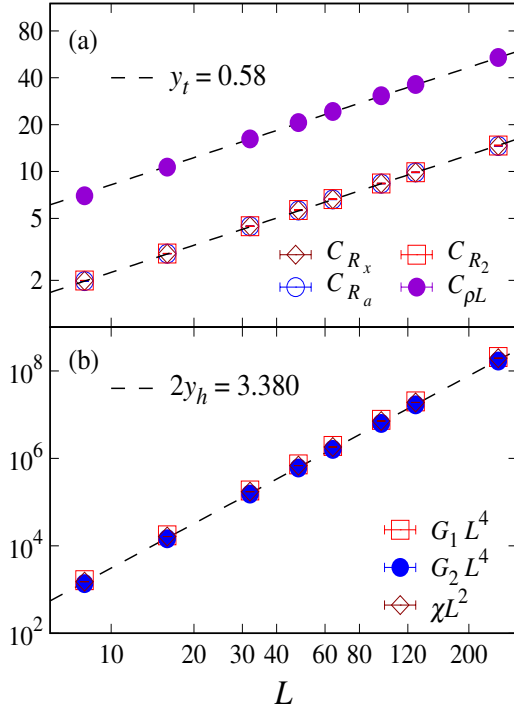


Figure 3. The dependence of quantities on L at the special transition. (a) Log-log plot of the covariances C_{R_x} , C_{R_a} , C_{R_2} and $C_{\rho L}$ versus L . The slope of dashed lines stands for $y_t = 0.58$. (b) Log-log plot of the scaled quantities $G_1 L^4$, $G_2 L^4$ and χL^2 versus L . The slope of dashed line stands for $2y_h = 3.380$.

a scale invariance point can be located at $\kappa_c \approx 0.441$, after properly handling finite-size corrections.

From the fitting results for R_x , R_a and ρ , the final estimate of κ_c is given as $\kappa_c = 0.44140(9)$. Meanwhile, the estimate of y_t is $y_t = 0.59(4)$, which agrees with the results 0.608(4) [6], 0.59(1) [26] and 0.61(2) [27] from various contexts of O(2) special SC, yet it suffers from larger uncertainty. A more precise determination of y_t will be given in the following subsection.

B. Universality class

We explore the universality class for the special transition, by computing y_t and y_h . We turn to FSS analyses right at $\kappa_c = 0.44140$, which have a reduced number of fitting parameters.

To estimate y_t , we consider the covariances C_O for dimensionless quantities ($O = R_x, R_a, R_2, \rho L$). According to Eq. (26), C_O scales as

$$C_O = L^{y_t} \tilde{C}_O(\epsilon L^{y_t}) \quad (30)$$

around κ_c . A fitting ansatz at κ_c reads

$$C_O = L^{y_t}(a_0 + b_1 L^{-\omega_1}), \quad (31)$$

where $b_1 L^{-\omega_1}$ is the leading term for finite-size corrections. Log-log plots of critical covariances versus L are shown in Fig. 3(a), which indicates the power-law scaling L^{y_t} . We perform fits to formula (31), considering the situations with leading correction term ($\omega_1 = 1$) or without finite-size correction. The results are presented in Table III. For each of the covariances, we obtain reasonable fits in the large-size regime, even when the correction term is absent. At $L_{\min} = 32$, we obtain $y_t = 0.573(2)$, $0.572(2)$, $0.574(3)$ and $0.580(2)$ with $\chi^2/\text{DoF} \approx 0.5, 0.3, 0.9$ and 1.1 , for C_{R_x} , C_{R_a} , C_{R_2} and $C_{\rho L}$, respectively. Finally, from Table III, our estimate of y_t is $y_t = 0.58(1)$.

With $y_t = 0.58$ and $\kappa_c = 0.44140$, Figs. 2(d), (e) and (f) display dimensionless quantities versus $(\kappa - \kappa_c)L^{y_t}$. According to Eqs. (26) and (28), the data collapses in the plots are indicators of reasonability for the estimated y_t and κ_c .

We perform FSS analyses for the surface quantities G_1 , G_2 and χ , from which y_h is estimated. The special transition features the power-law scaling and the critical two-point correlation obeys

$$g(r) \sim r^{2y_h-4} \quad (32)$$

at κ_c . Hence, the FSS for G_1 and G_2 is described by

$$G = L^{2y_h-4}(a_0 + b_1 L^{-\omega_1}). \quad (33)$$

Since χ scales as $\chi = L^{2y_h-2}\tilde{\chi}(\epsilon L^{y_t})$, its FSS at κ_c is written as

$$\chi = L^{2y_h-2}(a_0 + b_1 L^{-\omega_1}). \quad (34)$$

The L^{2y_h} divergence for scaled quantities $G_1 L^4$, $G_2 L^4$ and χL^2 is illustrated by Fig. 3(b). According to Eqs. (33) and (34), the fits for G_1 , G_2 and χ are performed. The results are given in Table IV. The estimates for ω_1 are close to $\omega_1 = 1$, as found in Sec. IV A. We note that, from each of the quantities G_1 , G_2 and χ , the fitting results of y_h by letting ω_1 be free (for smaller L_{\min} , namely $L_{\min} = 8$) and letting $\omega_1 = 1$ be fixed (for larger L_{\min} , namely $L_{\min} = 48$) are all compatible with $y_h \approx 1.690$. For G_1 and χ , preferred fits are found with the cutoffs $L_{\max} = 128$ and 256 . For G_2 , precluding input data at $L = 256$, which suffers from large relative statistical errors, is useful for improving the quality of fits. As a result, for $L_{\max} = 128$, we obtain $y_h = 1.690(1)$, $1.6901(2)$ and $1.6900(4)$ with $\chi^2/\text{DoF} \approx 1.7, 1.3$ and 1.7 , respectively. By comparing the fits in Table IV, the final estimate of y_h is $y_h = 1.690(1)$.

V. EXTRAORDINARY-LOG CRITICAL PHASE

A. Two-point correlation

To probe ELU, we perform extensive simulations in the deep extraordinary regime with $\kappa = 5$ and 10 , and obtain precise Monte Carlo data for G_1 and G_2 . According to Eq. (2),

Table V. Fits of the two-point correlations G_1 and G_2 to Eq. (35) for the extraordinary critical phase.

\mathcal{Q}	κ	L_{\min}	χ^2/DoF	a	c	\hat{q}
G_1	5	8	31.45/5	2.74(1)	5.52(2)	0.579(1)
		16	3.08/4	2.80(2)	5.65(3)	0.586(2)
		32	1.76/3	2.77(3)	5.59(6)	0.583(3)
		48	0.13/2	2.72(5)	5.50(9)	0.578(5)
		64	0.11/1	2.72(7)	5.5(1)	0.577(8)
	10	8	43.83/5	3.60(4)	10.60(8)	0.541(3)
		16	2.61/4	3.87(6)	11.1(1)	0.561(4)
		32	1.93/3	4.0(1)	11.3(2)	0.566(8)
		48	1.54/2	4.0(2)	11.5(4)	0.57(1)
		64	0.46/1	4.3(3)	11.9(6)	0.59(2)
G_2	5	8	6.22/5	2.84(2)	6.09(3)	0.590(2)
		16	3.15/4	2.81(2)	6.02(5)	0.587(3)
		32	1.38/3	2.76(4)	5.93(8)	0.582(5)
		48	0.24/2	2.71(7)	5.8(1)	0.576(7)
		64	0.15/1	2.7(1)	5.8(2)	0.57(1)
	10	8	5.46/5	3.95(6)	11.6(1)	0.566(4)
		16	5.27/4	3.92(8)	11.6(2)	0.564(6)
		32	5.16/3	3.9(1)	11.5(3)	0.56(1)
		48	4.13/2	4.1(2)	11.9(4)	0.57(2)
		64	0.12/1	4.6(5)	12.9(7)	0.61(3)

Table VI. Fits of the susceptibility χ to Eq. (36) for the extraordinary critical phase.

κ	L_{\min}	χ^2/DoF	a	c	\hat{q}
5	16	23.43/4	2.93(2)	6.06(3)	0.600(2)
	32	3.35/3	2.80(3)	5.82(6)	0.586(4)
	48	1.45/2	2.75(5)	5.7(1)	0.580(5)
	64	1.39/1	2.74(8)	5.7(1)	0.579(8)
	16	5.16/4	4.17(7)	11.9(1)	0.580(5)
10	32	4.35/3	4.1(1)	11.7(2)	0.574(8)
	48	2.68/2	4.3(2)	12.1(4)	0.59(1)
	64	0.002/1	4.7(4)	12.7(6)	0.61(2)

the FSS formula of G_1 and G_2 is written as

$$G = a[(\ln L) + c]^{-\hat{q}} \quad (35)$$

with c a non-universal constant. We perform fits for G_1 and G_2 , with the results being summarized in Table V. At $\kappa = 5$, the fits for G_1 are stable if $L_{\min} \gtrsim 16$, producing $\hat{q} = 0.586(2)$ and $0.583(3)$ with $\chi^2/\text{DoF} \approx 0.8$ and 0.6 , respectively. Comparatively, the finite-size G_2 data are more compatible to Eq. (35) for $L_{\min} = 8$. Preferred fits with $\chi^2/\text{DoF} \approx 1$ yield $\hat{q} = 0.590(2)$, $0.587(3)$ and $0.582(5)$ for $L_{\min} = 8, 16$ and 32 , respectively. At $\kappa = 10$, we obtain $\hat{q} = 0.561(4)$, $0.566(8)$, $0.57(1)$ and $0.59(2)$ for G_1 , as well as $\hat{q} = 0.566(4)$, $0.564(6)$ and $0.56(1)$ for G_2 . These estimates agree within error bars with the previous estimate $\hat{q} = 0.59(2)$ from classical XY model [24], providing strong evidence for the existence of ELU in OSV model.

From Eq. (2), we obtain a FSS formula for χ , which reads

$$\chi = aL^2[(\ln L) + c]^{-\hat{q}}, \quad (36)$$

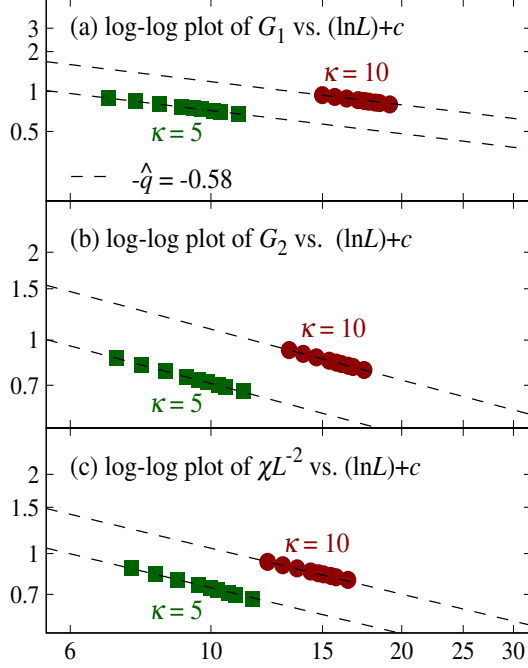


Figure 4. Log-log plot of G_1 (a), G_2 (b) and χL^{-2} (c) versus $(\ln L) + c$. The dashed lines stand for the critical scaling $(\ln L)^{-\hat{q}}$ with $\hat{q} = 0.58$. The constant c is non-universal and comes from the preferred least-squares fits of G_1 and G_2 to Eq. (35) or χ to Eq. (36).

due to $\chi \sim \int g(r) r dr$. Table VI displays the existence of preferred fits to Eq. (36) for $\kappa = 5$ and 10. For $\kappa = 5$, we have the fitting results $\hat{q} = 0.586(4)$, $0.580(5)$ and $0.579(8)$ with $\chi^2/\text{DoF} \approx 1.1$, 0.7 and 1.4 , for $L_{\min} = 32, 48$ and 64 , respectively. For $\kappa = 10$, we obtain $\hat{q} = 0.580(5)$, $0.574(8)$ and $0.59(1)$ with $\chi^2/\text{DoF} \approx 1.3$, 1.5 and 1.3 , for $L_{\min} = 16, 32$ and 48 , respectively. Therefore, the estimates of \hat{q} from χ are compatible with the results from G_1 and G_2 .

Generally speaking, the FSS analysis involving $\ln L$ is difficult. Hence, the stability of fits is examined by varying L_{\min} and we do not trust any single fit even though the chi-squared criterion is satisfied. The estimates of fitting parameters (including \hat{q}) arise from a comparison of the fits with different L_{\min} . Moreover, to monitor the corrections to scaling, we systematically compare the estimates of \hat{q} from various quantities. We also compare the results from different interaction strengths in the extraordinary-log regime. A similar procedure was applied in a previous study [24], of which the estimate of \hat{q} has been confirmed by independent studies in various contexts (Table I). Here, by comparing the preferred fits for G_1 , G_2 and χ , we estimate $\hat{q} = 0.58(2)$. By adopting the parameter c from the fits, we plot G_1 , G_2 and χL^{-2} versus $(\ln L) + c$ in Fig. 4, which illustrates mutually consistent results for universal and non-universal parameters.

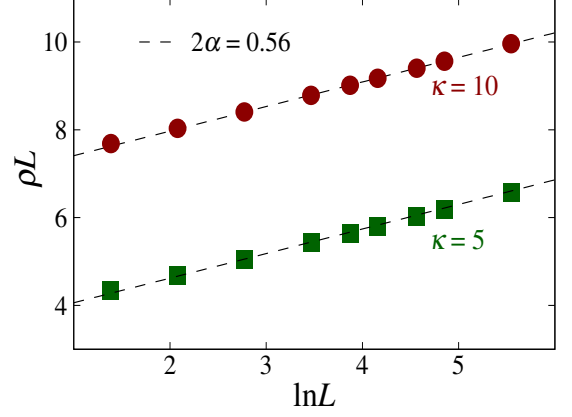


Figure 5. The scaled SF stiffness ρL versus $\ln L$. The dashed lines stand for 2α .

Table VII. Fits of the SF stiffness ρ to Eq. (37) for the extraordinary critical phase. The underlines denote that the data for $L = 128$ are not included in fitting.

κ	L_{\min}	L_{\max}	χ^2/DoF	α	b
5	32	256	32.11/4	0.2770(4)	3.498(3)
	48	256	5.38/3	0.2785(5)	3.484(4)
	64	256	3.87/2	0.2790(6)	3.479(6)
	96	256	0.79/1	0.280(1)	3.47(1)
	32	128	18.79/3	0.2756(5)	3.509(4)
	48	128	3.15/2	0.2776(7)	3.491(6)
	64	128	2.91/1	0.278(1)	3.49(1)
	<u>32</u>	<u>256</u>	32.08/3	0.2769(4)	3.499(4)
	<u>48</u>	<u>256</u>	5.38/2	0.2785(5)	3.484(5)
	<u>64</u>	<u>256</u>	3.87/1	0.2790(7)	3.479(6)
10	32	256	7.35/4	0.2822(6)	6.827(5)
	48	256	6.28/3	0.2828(8)	6.821(8)
	64	256	4.13/2	0.284(1)	6.81(1)
	96	256	3.51/1	0.285(2)	6.80(1)
	32	128	1.13/3	0.2810(8)	6.837(7)
	48	128	1.10/2	0.281(1)	6.84(1)
	64	128	1.03/1	0.281(2)	6.83(2)
	<u>32</u>	<u>256</u>	3.23/3	0.2828(7)	6.823(6)
	<u>48</u>	<u>256</u>	1.85/2	0.2835(9)	6.816(8)
	<u>64</u>	<u>256</u>	0.05/1	0.284(1)	6.81(1)

B. Superfluid stiffness

We examine the analogy of ρ to the SF stiffness of open-edge Bose-Hubbard model considered in Ref. [28], where it was defined through the winding number fluctuations in path-integral world-line representation. As shown in Fig. 5, there is a linear divergence of ρL on $\ln L$. The renormalization-group universal parameter α controls the FSS of ρ , which can be written as

$$\rho L = 2\alpha(\ln L) + b. \quad (37)$$

Estimates of α come from the fits of ρ to Eq. (37), which are summarized in Table VII. For $\kappa = 5$, we obtain $\alpha =$

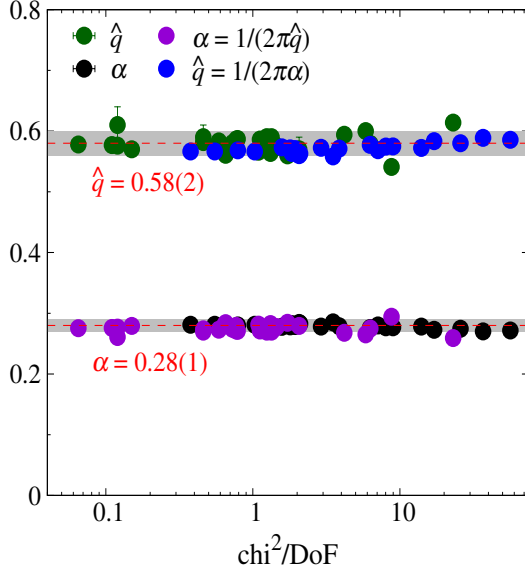


Figure 6. Verification for the scaling relation (4) with $N = 2$. The green and black symbols with error bars stand for fitting results from FSS analyses, while the purple and blue symbols without error bars are transformed from the fitting results via the relation $\alpha\hat{q} = 1/(2\pi)$. The shadowed areas centered at dashed red lines denote the critical exponent $\hat{q} = 0.58(2)$ and the renormalization-group parameter $\alpha = 0.28(1)$.

0.2785(5), 0.2790(6) and 0.280(1) with $\chi^2/\text{DoF} \approx 1.8$, 1.9 and 0.8, for $L_{\min} = 48$, 64 and 96, respectively. We are aware of the price of including large-size data with relatively large uncertainties, and also perform fits with $L = 256$ being precluded, i.e., $L_{\max} = 128$. As a result, we obtain $\alpha = 0.2776(7)$ and 0.278(1) with $\chi^2/\text{DoF} \approx 1.6$ and 2.9, respectively. Then, we perform fits with the second-largest size $L = 128$ being precluded yet $L = 256$ being contained, for which the residuals are larger. A similar fitting procedure is applied to $\kappa = 10$, and preferred fits are achieved. For $L_{\max} = 128$, we obtain 0.2810(8), 0.281(1) and 0.281(2) with $\chi^2/\text{DoF} \approx 0.4$, 0.6 and 1.0, respectively. When $L = 128$ is precluded yet $L = 256$ is contained, we obtain 0.2828(7) and 0.2835(9) with $\chi^2/\text{DoF} \approx 1.1$ and 0.9, respectively. Therefore, the estimates of α from $\kappa = 5$ and 10 are close to each other. By comparing the fitting results in Table VII, the universal value of α is estimated to be $\alpha = 0.28(1)$.

C. Scaling relation

We proceed to verify the scaling relation (4) of the critical exponent \hat{q} and the renormalization-group parameter α . Figure 6 demonstrates the fitting results for \hat{q} and α versus χ^2/DoF , which are quoted from Tables V, VI and VII.

In the plot, the two shadowed areas with $\hat{q} = 0.58(2)$ and $\alpha = 0.28(1)$ denote the final estimates from fitting. Next, using scaling relation (4) with $N = 2$, namely $\alpha\hat{q} = 1/(2\pi)$, we obtain estimates of α and \hat{q} from each other, and the results are also presented in Fig. 6. It is found that the estimates of \hat{q} and α from scaling relation are close to the final estimates indicated by shadowed areas, particularly when $\chi^2/\text{DoF} \approx 1$ is approached. Hence, the scaling relation (4) is compatible with present numerical results.

VI. DISCUSSION

To bridge the recent observations of exotic SC in classical statistical mechanical models [23–25] and quantum Bose-Hubbard model [28], we formulate the OSV model for special and extraordinary-log criticality, which is extensively simulated by a worm Monte Carlo algorithm. For the special transition, the thermal and magnetic renormalization exponents are estimated to be $y_t = 0.58(1)$ and $y_h = 1.690(1)$ respectively, which are consistent with recent results from classical spin models of emergent O(2) criticality [26, 27]. For the extraordinary-log phase, the critical exponent \hat{q} and the universal renormalization-group parameter α are estimated to be $\hat{q} = 0.58(2)$ and $\alpha = 0.28(1)$, which are compatible with scaling relation (4) with $N = 2$. Meanwhile, the estimated \hat{q} and α are fully consistent with previous results from XY model [24]. Moreover, the SF stiffness scales as L^{-1} at the special transition and as $L^{-1}(\ln L)$ for the extraordinary-log critical phase. These features resemble the scaling formulae of SF stiffness for open-edge quantum Bose-Hubbard model [28], where the stiffness was sampled over world-line configurations. Hence, the present work provides an alternative demonstration for ELU and bridges recent numerical observations over classical and quantum SC. As a byproduct, it is promising that the quantitative results for special and extraordinary-log criticality would serve as a long-standing benchmark.

One direction for future work may be to finely tune the geometries of boundaries for a critical Bose-Hubbard or Villain system by employing a full Suzuki-Trotter-type limiting procedure that underlies the quantum-classical correspondence. Such an activity would offer a routine to reconcile the current questions about SC in dimerized quantum antiferromagnets [10–14, 38–40], where the emergence of SC subtly depends on geometric settings of boundaries and relates to symmetry-protected topological phases.

ACKNOWLEDGMENTS

One of us (J.P.L.) wishes to thank Youjin Deng and Minghui Hu for the collaboration in an earlier study [24]. The present work has been supported by the National Natural Science Foundation of China (under Grant Nos. 12275002, 11975024, and 11774002) and the Education Department of Anhui.

-
- [1] K. Binder and P. C. Hohenberg, “Surface effects on magnetic phase transitions,” *Phys. Rev. B* **9**, 2194 (1974).
- [2] K. Ohno and Y. Okabe, “The $1/n$ expansion for the extraordinary transition of semi-infinite system,” *Prog. Theor. Phys.* **72**, 736–745 (1984).
- [3] D. P. Landau, R. Pandey, and K. Binder, “Monte carlo study of surface critical behavior in the xy model,” *Phys. Rev. B* **39**, 12302 (1989).
- [4] H. W. Diehl, “The theory of boundary critical phenomena,” *Int. J. Mod. Phys. B* **11**, 3503–3523 (1997), [arXiv:cond-mat/9610143 \[cond-mat\]](#).
- [5] M. Pleimling, “Critical phenomena at perfect and non-perfect surfaces,” *J. Phys. A: Math. and Gen.* **37**, R79 (2004), [arXiv:cond-mat/0402574 \[cond-mat\]](#).
- [6] Y. Deng, H. W. J. Blöte, and M. P. Nightingale, “Surface and bulk transitions in three-dimensional $o(n)$ models,” *Phys. Rev. E* **72**, 016128 (2005), [arXiv:cond-mat/0504173 \[cond-mat\]](#).
- [7] Y. Deng, “Bulk and surface phase transitions in the three-dimensional $o(4)$ spin model,” *Phys. Rev. E* **73**, 056116 (2006).
- [8] J. Dubail, J. L. Jacobsen, and H. Saleur, “Exact solution of the anisotropic special transition in the $o(n)$ model in two dimensions,” *Phys. Rev. Lett.* **103**, 145701 (2009), [arXiv:0909.2949 \[cond-mat\]](#).
- [9] M. Hasenbusch, “Monte carlo study of surface critical phenomena: The special point,” *Phys. Rev. B* **84**, 134405 (2011), [arXiv:1108.2425 \[cond-mat\]](#).
- [10] L. Zhang and F. Wang, “Unconventional surface critical behavior induced by a quantum phase transition from the two-dimensional affleck-kennedy-lieb-tasaki phase to a néel-ordered phase,” *Phys. Rev. Lett.* **118**, 087201 (2017), [arXiv:1611.06477 \[cond-mat\]](#).
- [11] C. Ding, L. Zhang, and W. Guo, “Engineering surface critical behavior of $(2+1)$ -dimensional $o(3)$ quantum critical points,” *Phys. Rev. Lett.* **120**, 235701 (2018), [arXiv:1801.10035 \[cond-mat\]](#).
- [12] L. Weber, F. Parisen Toldin, and S. Wessel, “Nonordinary edge criticality of two-dimensional quantum critical magnets,” *Phys. Rev. B* **98**, 140403(R) (2018), [arXiv:1804.06820 \[cond-mat\]](#).
- [13] L. Weber and S. Wessel, “Nonordinary criticality at the edges of planar spin-1 heisenberg antiferromagnets,” *Phys. Rev. B* **100**, 054437 (2019), [arXiv:1906.07051 \[cond-mat\]](#).
- [14] C.-M. Jian, Y. Xu, X.-C. Wu, and C. Xu, “Continuous neel-vbs quantum phase transition in non-local one-dimensional systems with $so(3)$ symmetry,” *SciPost Phys.* **10**, 033 (2021), [arXiv:2004.07852 \[cond-mat\]](#).
- [15] M. A. Metlitski, “Boundary criticality of the $o(n)$ model in $d=3$ critically revisited,” *SciPost Phys.* **12**, 131 (2022), [arXiv:2009.05119 \[cond-mat\]](#).
- [16] T. Grover and A. Vishwanath, “Quantum criticality in topological insulators and superconductors: Emergence of strongly coupled majoranas and supersymmetry,” [arXiv:1206.1332 \[cond-mat\]](#).
- [17] D. E. Parker, T. Scaffidi, and R. Vasseur, “Topological luttinger liquids from decorated domain walls,” *Phys. Rev. B* **97**, 165114 (2018), [arXiv:1711.09106 \[cond-mat\]](#).
- [18] S. Liu, H. Shapourian, A. Vishwanath, and M. A. Metlitski, “Magnetic impurities at quantum critical points: Large- n expansion and connections to symmetry-protected topological states,” *Phys. Rev. B* **104**, 104201 (2021), [arXiv:2104.15026 \[cond-mat\]](#).
- [19] D. M. Dantchev and S. Dietrich, “Critical casimir effect: Exact results,” [arXiv:2203.15050 \[cond-mat\]](#).
- [20] J. Cardy, “Boundary conformal field theory,” [arXiv:hep-th/0411189 \[cond-mat\]](#).
- [21] N. Andrei, A. Bissi, M. Buican, J. Cardy, P. Dorey, N. Drukker, J. Erdmenger, D. Friedan, D. Fursaev, A. Konechny, C. Kristjansen, I. Makabe, Y. Nakayama, A. O’Bannon, R. Parini, B. Robinson, S. Ryu, C. Schmidt-Colinet, V. Schomerus, C. Schweigert, and G. M. T. Watts, “Boundary and defect CFT: open problems and applications,” *J. Phys. A: Math. and Theo.* **53**, 453002 (2020), [arXiv:1810.05697 \[cond-mat\]](#).
- [22] J. Padayasi, A. Krishnan, M. A. Metlitski, I. A. Gruzberg, and M. Meineri, “The extraordinary boundary transition in the 3d $o(n)$ model via conformal bootstrap,” *SciPost Physics* **12**, 190 (2022), [arXiv:2111.03071 \[cond-mat\]](#).
- [23] F. Parisen Toldin, “Boundary critical behavior of the three-dimensional heisenberg universality class,” *Phys. Rev. Lett.* **126**, 135701 (2021), [arXiv:2012.00039 \[cond-mat\]](#).
- [24] M. Hu, Y. Deng, and J.-P. Lv, “Extraordinary-log surface phase transition in the three-dimensional xy model,” *Phys. Rev. Lett.* **127**, 120603 (2021), [arXiv:2104.05152 \[cond-mat\]](#).
- [25] F. Parisen Toldin and M. A. Metlitski, “Boundary criticality of the 3d $o(n)$ model: from normal to extraordinary,” *Phys. Rev. Lett.* **128**, 215701 (2022), [arXiv:2111.03613 \[cond-mat\]](#).
- [26] L.-R. Zhang, C. Ding, Y. Deng, and L. Zhang, “Surface criticality of the antiferromagnetic potts model,” *Phys. Rev. B* **105**, 224415 (2022), [arXiv:2204.11692 \[cond-mat\]](#).
- [27] X. Zou, S. Liu, and W. Guo, “Surface critical properties of the three-dimensional clock model,” *Phys. Rev. B* **106**, 064420 (2022), [arXiv:2204.13612 \[cond-mat\]](#).
- [28] Y. Sun and J.-P. Lv, “Quantum extraordinary-log universality of boundary critical behavior,” *Phys. Rev. B* **106**, 224502 (2022), [arXiv:2205.00878 \[cond-mat\]](#).
- [29] M. Wittmann and A. P. Young, “Finite-size scaling above the upper critical dimension,” *Phys. Rev. E* **90**, 062137 (2014), [arXiv:1410.5296 \[cond-mat\]](#).
- [30] E. Flores-Sola, B. Berche, R. Kenna, and M. Weigel, “Role of fourier modes in finite-size scaling above the upper critical dimension,” *Phys. Rev. Lett.* **116**, 115701 (2016), [arXiv:1511.04321 \[cond-mat\]](#).
- [31] V. Papathanakos, *Finite-size effects in high-dimensional statistical mechanical systems: The Ising model with periodic boundary conditions* (Ph.D. thesis, Princeton University, Princeton, New Jersey, 2006).
- [32] H. Shao, W. Guo, and A. W. Sandvik, “Quantum criticality with two length scales,” *Science* **352**, 213–216 (2016), [arXiv:1603.02171 \[cond-mat\]](#).
- [33] J. Grimm, E. M. Elçi, Z. Zhou, T. M. Garoni, and Y. Deng, “Geometric explanation of anomalous finite-size scaling in high dimensions,” *Phys. Rev. Lett.* **118**, 115701 (2017), [arXiv:1612.01722 \[cond-mat\]](#).
- [34] Z. Zhou, J. Grimm, S. Fang, Y. Deng, and T. M. Garoni, “Random-length random walks and finite-size scaling in high dimensions,” *Phys. Rev. Lett.* **121**, 185701 (2018), [arXiv:1809.00515 \[cond-mat\]](#).
- [35] S. Fang, J. Grimm, Z. Zhou, and Y. Deng, “Complete graph and gaussian fixed-point asymptotics in the five-dimensional fortuin-kasteleyn ising model with periodic boundaries,” *Phys. Rev. E* **102**, 022125 (2020), [arXiv:1909.04328 \[cond-mat\]](#).
- [36] J.-P. Lv, W. Xu, Y. Sun, K. Chen, and Y. Deng, “Finite-size scaling of $o(n)$ systems at the upper critical dimensionality,” *Nat. Sci. Rev.* **8**, nwaa212 (2021), [arXiv:1909.10347 \[cond-](#)

- mat].
- [37] M. E. Fisher, M. N. Barber, and D. Jasnow, “Helicity modulus, superfluidity, and scaling in isotropic systems,” *Phys. Rev. A* **8**, 1111–1124 (1973).
 - [38] L. Weber and S. Wessel, “Spin versus bond correlations along dangling edges of quantum critical magnets,” *Phys. Rev. B* **103**, L020406 (2021), [arXiv:2010.15691 \[cond-mat\]](#).
 - [39] W. Zhu, C. Ding, L. Zhang, and W. Guo, “Exotic surface behaviors induced by geometrical settings of two-dimensional dimerized quantum xxz model,” [arXiv:2111.12336 \[cond-mat\]](#).
 - [40] C. Ding, W. Zhu, W. Guo, and L. Zhang, “Special transition and extraordinary phase on the surface of a $(2+1)$ -dimensional quantum heisenberg antiferromagnet,” [arXiv:2110.04762 \[cond-mat\]](#).
 - [41] W. Witczak-Krempa, E. S. Sørensen, and S. Sachdev, “The dynamics of quantum criticality revealed by quantum monte carlo and holography,” *Nat. Phys.* **10**, 361 (2014), [arXiv:1309.2941 \[cond-mat\]](#).
 - [42] M. P. A. Fisher, P. B. Weichman, G. Grinstein, and D. S. Fisher, “Boson localization and the superfluid-insulator transition,” *Phys. Rev. B* **40**, 546 (1989).
 - [43] H. Zhai, *Ultracold Atomic Physics* (Cambridge University Press, 2021).
 - [44] M. P. A. Fisher and G. Grinstein, “Quantum critical phenomena in charged superconductors,” *Phys. Rev. Lett.* **60**, 208–211 (1988).
 - [45] M. Wallin, E. S. Sørensen, S. M. Girvin, and A. P. Young, “Superconductor-insulator transition in two-dimensional dirty boson systems,” *Phys. Rev. B* **49**, 12115–12139 (1994).
 - [46] J. Villain, “Theory of one-and two-dimensional magnets with an easy magnetization plane. ii. the planar, classical, two-dimensional magnet,” *J. de Phys. (Paris)* **36**, 581–590 (1975).
 - [47] J. Kisker and H. Rieger, “The two-dimensional disordered boson hubbard model: Evidence for a direct mott-insulator-to-superfluid transition and localization in the bose glass phase,” *Physica A: Statistical Mechanics and its Applications* **246**, 348–376 (1997), [arXiv:cond-mat/9703149 \[cond-mat\]](#).
 - [48] M. C. Cha, M. P. A. Fisher, S. M. Girvin, M. Wallin, and A. P. Young, “Universal conductivity of two-dimensional films at the superconductor-insulator transition,” *Phys. Rev. B* **44**, 6883 (1991).
 - [49] F. Alet and E. S. Sørensen, “Cluster monte carlo algorithm for the quantum rotor model,” *Phys. Rev. E* **67**, 015701(R) (2003), [arXiv:cond-mat/0211262 \[cond-mat\]](#).
 - [50] J. Šmakov and E. Sørensen, “Universal scaling of the conductivity at the superfluid-insulator phase transition,” *Phys. Rev. Lett.* **95**, 180603 (2005), [arXiv:cond-mat/0509671 \[cond-mat\]](#).
 - [51] K. Chen, L. Liu, Y. Deng, L. Pollet, and N. Prokof’ev, “Universal conductivity in a two-dimensional superfluid-to-insulator quantum critical system,” *Phys. Rev. Lett.* **112**, 030402 (2014), [arXiv:1309.5635 \[cond-mat\]](#).
 - [52] P. Dario and W. Wu, “Massless phases for the villain model in $d \geq 3$,” *Preprint* (2020).
 - [53] W. Xu, Y. Sun, J.-P. Lv, and Y. Deng, “High-precision monte carlo study of several models in the three-dimensional $u(1)$ universality class,” *Phys. Rev. B* **100**, 064525 (2019), [arXiv:1908.10990 \[cond-mat\]](#).
 - [54] N. V. Prokof’ev and B. V. Svistunov, “Worm algorithms for classical statistical models,” *Phys. Rev. Lett.* **87**, 160601 (2001), [arXiv:cond-mat/0103146 \[cond-mat\]](#).
 - [55] J. Lyu, *Monte Carlo simulations of the open-surface Villain model and the semi-hard-core bosonic model* (Master thesis, Anhui Normal University, Wuhu, Anhui, 2022).
 - [56] Y. Deng, T. M. Garoni, and A. D. Sokal, “Dynamic critical behavior of the worm algorithm for the ising model,” *Phys. Rev. Lett.* **99**, 110601 (2007), [arXiv:cond-mat/0703787 \[cond-mat\]](#).
 - [57] W. Zhang, T. M. Garoni, and Y. Deng, “A worm algorithm for the fully-packed loop model,” *Nucl. Phys. B* **814**, 461–484 (2009), [arXiv:0811.2042 \[cond-mat\]](#).
 - [58] J.-P. Lv, Y. Deng, and Q.-H. Chen, “Worm-type monte carlo simulation of the ashkin-teller model on the triangular lattice,” *Phys. Rev. E* **84**, 021125 (2011), [arXiv:1009.3172 \[cond-mat\]](#).
 - [59] Practically, this can be realized alternatively by setting pseudo edges between the two open surfaces, which have zero relative statistical weights for finite \mathcal{J} with respect to $\mathcal{J} = 0$.
 - [60] R. P. Langlands, C. Pichet, P. Pouliot, and Y. Saint-Aubin, “On the universality of crossing probabilities in two-dimensional percolation,” *J. Stat. Phys.* **67**, 553–574 (1992).
 - [61] H. T. Pinson, “Critical percolation on the torus,” *J. Stat. Phys.* **75**, 1167–1177 (1994).
 - [62] R. M. Ziff, C. D. Lorenz, and P. Kleban, “Shape-dependent universality in percolation,” *Physica A* **266**, 17–26 (1999).
 - [63] J. Wang, Z. Zhou, W. Zhang, T. M. Garoni, and Y. Deng, “Bond and site percolation in three dimensions,” *Phys. Rev. E* **87**, 052107 (2013), [arXiv:1302.0421 \[cond-mat\]](#).
 - [64] X. Xu, J. Wang, J.-P. Lv, and Y. Deng, “Simultaneous analysis of three-dimensional percolation models,” *Front. Phys.* **9**, 113–119 (2014), [arXiv:1310.5399 \[cond-mat\]](#).
 - [65] M. Hu, Y. Sun, D. Wang, J.-P. Lv, and Y. Deng, “History-dependent percolation in two dimensions,” *Phys. Rev. E* **102**, 052121 (2020), [arXiv:2005.12035 \[cond-mat\]](#).
 - [66] B.-Z. Wang, P. Hou, C.-J. Huang, and Y. Deng, “Percolation of the two-dimensional xy model in the flow representation,” *Phys. Rev. E* **103**, 062131 (2021), [arXiv:1108.2425 \[cond-mat\]](#).
 - [67] R. Guida and J. Zinn-Justin, “Critical exponents of the n -vector model,” *J. Phys. A: Math. Gen.* **31**, 8103 (1998), [arXiv:cond-mat/9803240 \[cond-mat\]](#).